Feasibility Studies of Parametric X-rays Use in a Medical Environment

Bryndol Sones[1], Yaron Danon[2], Ezekiel Blain[2]

1. *Department of Physics, United States Military Academy, ATTN: MADN-PHYS, 646 Swift Road, West Point NY 10996-1905, United States*
2. *Department of Mechanical, Aerospace and Nuclear Engineering, Rensselaer Polytechnic Institute, 110 8th St., Troy NY 12180, United States*

Abstract. Parametric X-rays (PXR) are produced from the interaction of relativistic electrons with the periodic structure of crystal materials. Smooth X-ray energy tunability is achieved by rotating the crystal with respects to the electron beam direction. Experiments at the Rensselaer Polytechnic Institute 60-MeV LINAC produce quasi-monochromatic X-rays (6-35 keV) from various target crystals to include highly oriented pyrolytic graphite (HOPG), LiF, Si, Ge, Cu, and W using electron beam currents up to 6 uA. These experiments demonstrate the first PXR images and some of the merits of thin metallic crystals. Recent experiments with a 100-μm thick Cu crystal improve the Cu PXR (with energy ~12 keV) to Cu fluorescence ratio by a factor of 20 compared to a 1 mm-thick Cu crystal. This study uses Monte Carlo techniques to investigate (1) PXR dose compared to emissions from simulated Mo, Rh, and W anodes for mammography applications and (2) electron scattering effects when considering LiF111, Si111, and Cu111 PXR production using electron beams with energies of 20-30 MeV. Advantages in using monochromatic PXR compared to X-rays from Mo and Rh anodes in mammography applications result in a dose per incident photon reduction by a factor of 2. Using 20 MeV electrons, the thinner Cu111 crystal for 15 keV PXR production results in an electron scattering angle of 30.7 +/- 0.2 mrad offering the best potential for PXR from lower energy electrons.

Keywords: LINAC, parametric X-ray, crystal, scattering, dose
PACS: 29.17.+w

INTRODUCTION

Novel X-ray sources such as channeling radiation (CR), diffracted transition radiation (DTR), coherent bremsstrahlung radiation (CBR), and parametric X-rays (PXR) are derived from relativistic electrons interacting with targets having a periodic structure. While each source has its own unique characteristics, they are particularly promising for imaging applications because of their spectral brightness, narrow energy linewidth, and, in the case of PXR, energy tunability [1, 2]. Recognizing their imaging potential and medical need, the U.S. National Institute of Biomedical Imaging and Bioengineering Health formed in 2000 has called attention to developing emerging novel X-ray technology for the health industry [3].

Parametric X-rays (PXR) may be described as the diffraction of "virtual photons" from crystal planes in the same manner that Bragg's Law governs X-ray diffraction. Numerous PXR experimental studies have been conducted using target crystals of Si, LiF, Ge, highly oriented pyrolytic graphite (HOPG), and W [4, 5, 6, 7]. PXR experiments at Rensselaer Polytechnic Institute (RPI) and at Lebra Facility in Japan produced X-ray images using PXR generated from 60 MeV and 100 MeV electrons, respectively [8, 9].

The objective of this study is to consider the use of PXR as an X-ray imaging source using existing medical resources. In particular, initial steps are taken (1) to compare the patient dose when using a quasi-monochromatic PXR compared to the emission from traditional anodes used in X-ray machines and (2) to determine the electron scattering effects when using lower energy electron accelerators (~ 20 MeV) such as those used for radiotherapy.

PXR THEORY

The energy of PXR is effectively independent of the electron incident energy and relies on the target crystal plane spacing and experimental geometry. Energy tunability is achieved by simply rotating the crystal [10]. The emission of PXR from a target crystal

CP1099, *Application of Accelerators in Research and Industry: 20th International Conference*
edited by F. D. McDaniel and B. L. Doyle

is confined to the small cone defined by the Lorentz factor, γ, of the incident electrons. The angle between the electron direction and the crystal planes is the Bragg angle, θ_B. The PXR photon distribution is described by $N(\theta_x, \theta_y)$ around the emission direction of $2\theta_B$ from the electron direction [11].

$$N(\theta_x,\theta_y) = \frac{{\theta_x}^2 \cos^2 2\theta_B + {\theta_y}^2}{({\theta_x}^2 + {\theta_y}^2 + {\theta_{ph}}^2)^2} \qquad (1)$$

where θ_x and θ_y are angular position coordinates, and θ_{ph} is approximately one over the Lorentz factor. Crystal mosaicity and electron scattering in the crystal cause adverse broadening of this photon distribution. Potylitsin proposes an geometric model to calculate these broadening effects which effectively fills the characteristic hole in the PXR photon distribution [12]. Figure 1 shows generic calculations of these effects for electron scattering as a factor of the characteristics angle, θ_{ph} [13].

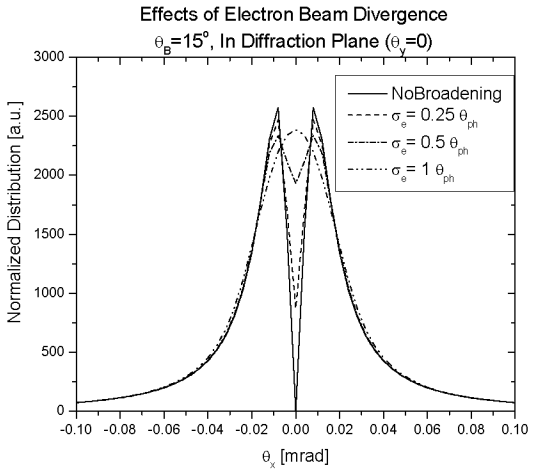

Figure 1. Electron divergence effects on PXR photon distribution. Calculations done as a function of θ_x with θ_{ph} = 8.5 mrad (60 MeV electrons), θ_y = 0, θ_B = 15°, no crystal mosaicity (σ_m=0), and varying values of σ_e = (0,0.25, 0.5, 1.0)* θ_{ph}.

THIN CU TARGET CRYSTALS

Target crystal thickness affects the amount of electron scattering. Thinner is better. Crystal thicknesses can be optimized to maximize PXR production and minimize PXR absorption. For crystals in the Bragg geometry, the optimized thickness is approximately one X-ray absorption length, L_a, in the target crystal [4]. For metallic crystals, this allows reduced thickness compared to common crystals such as Si and LiF. Metal fluorescence noise might compete with the PXR, but in recent RPI experiments the ratio of PXR to K_α fluorescence was increased by a factor of 20 by using a 1-um thick Cu crystal compared to earlier experiments using a 1-mm thick crystal [14]. This was the first experimental realization of Cu111 PXR. This is a promising result since metallic crystals will likely be more durable for imaging applications where higher electron beam current are necessary. Both Si and LiF crystals have fractured under high electron beam currents [8, 9].

MAMMOGRAPHY PATIENT DOSE

High electron beam currents are not issues for existing medical X-ray machines because they use a robust and sometimes cooled metallic anode interacting with electrons with energies in the 100 keV range depending on the body part to image [15]. Even with filtering and collimation, the X-ray spectrum is inherently polychromatic while the predominant X-ray employed for the image is the fluorescence from the target anode. For mammography, the anodes are typically Mo or Rh which have K_α fluorescence at 17.48 keV and 20.21 keV, respectively [15]. Monte-Carlo techniques (MCNPX F1 tallies) generate the X-ray source terms when 100 keV electrons are incident at 45° to Mo and Rh anodes [16]. Breasts are modeled in a simple geometry as hemispheres (spheres sliced in a vertical plane) with radii consistent with A, B, C, and D cup bra sizes and with material composition of breast tissue from ICRU #44 [17]. Breasts are not compressed as in a mammography machine so not to affect the material density. To compare dose, MCNPX F6 tallies generate the energy deposited in the modeled breast. The anode source terms are defined into 20 energy/probability bins in the F6 tally. Similar F6 tallies are done with monochromatic 17.48 keV and 20.21 keV PXR. The output is total absorbed energy per photon. For the C cup size, the result for the Mo anode was 3583 ± 4 eV/photon compared to 1659 ± 4 eV/photon for the 17.48 MeV PXR. No significant difference is observed between other breast sizes. In the case of the Mo and Rh anodes, the PXR reduced the patient dose by a factor of two.

LOW ENERGY ELECTRON SOURCE

The Varian Clinac 2100 is used for the basis of this analysis. The Varian brand is ubiquitous in hospital radiotherapy, and this machine produces an electron beam with energy of 18 MeV [18]. For this feasibility study, the aim is to analyze the electron scattering in the target crystal. As discussed in the

PXR Theory, electron scattering broadens the PXR photon distribution and reduces its intensity. The evaluation metric is the electron beam divergence measured as the standard deviation, σ, of the beam profile as it exits the crystal; 2σ represents the profile full width half maximum (FWHM) of a Gaussian distribution. Three cubic crystals are considered: LiF111, Si111, and Cu111. This study examines PXR energies of 15 keV, 30 keV, 45 keV, and 60 keV from these crystals interacting with electrons with energies of 20 MeV, 25 MeV, 30 MeV, and 60 MeV. With MCNPX, F1 tallies were made using a pencil beam electron source incident normal to the target crystal whose thickness was varied to optimize PXR production at the given PXR energies. These target thicknesses were chosen as one X-ray absorption length, *La*, in the target crystal. The F1 tallies produced 1,000 angular bins of cosine of the electron deflection angle from 0.99 to 1. This data was assumed symmetric and folded over to produce the electron angular distribution which was fitted to a Gaussian function using Origin Version 7.5. Representative distributions for scattering of 20 MeV electrons in the three crystals with thicknesses for 15 keV PXR are shown in Figure 2. The differences in the electron scattering are primarily attributed to the differences in the target crystal thicknesses. Table I summarizes the results of electron scattering study as well as a comparison of the target thickness and the electron CSDA range [17]. When the target thickness, *t*, approaches the CSDA Range, there is reason for concern. This is shown as the ratio of *t* to CSDA Range. Ratio values >0.1 complicate PXR production with heat deposition and make these MCNPX calculations futile as shown with the * in the table. The other important feature in the table is the ratio of the electron scattering σ to the PXR characteristic angle, θ_{ph}. Successful PXR experiments at RPI have been done with the ratio as big as 6, but this was done with 60 MeV electrons. Since the PXR distribution broadening model [12] is geometric, one might expect the model to be valid at lower electron energies. Nonetheless, the higher LiF σ to θ_{ph} ratios casts suspicion on LiF use for higher energy PXR production while the lower Cu σ to θ_{ph} ratios offer some promise for its use at any of the selected PXR energies using electron energies as low as 20 MeV.

TABLE 1. Electron scattering results for 20 MeV, 25 MeV, and 30 MeV electrons incident on Cu111, Si111, LiF111 PXR targets with thickness, t, of one absorption length, La, for the given PXR energies of 15 keV, 30 keV, and 45 keV.

Crystal Parameters	Electron Energy								
	20 MeV (θph=25.6 mrad)			25 MeV (θph=20.4 mrad)			30 MeV (θph=17.0 mrad)		
	PXR Energy								
	15 keV	30 keV	45 keV	15 keV	30 keV	45 keV	15 keV	30 keV	45 keV
Cu111 Crystal									
Ratio (t/CSDA Range)	1.3E-03	8.8E-03	2.7E-02	1.1E-03	7.5E-03	2.3E-02	9.8E-04	6.7E-03	2.1E-02
Scattering σ [mrad]	30.7+/- 0.2	84.2+/- 0.3	156.6+/- 0.8	23.4+/- 0.2	67.4+/- 0.3	129.8+/- 0.2	16.9+/- 0.2	57.8+/- 0.2	107.6+/- 0.1
Ratio σ/θph	1.2	3.3	6.1	1.1	3.3	6.3	1.0	3.4	6.3
Si111 Crystal									
Ratio (t/CSDA Range)	1.0E-02	8.3E-02	2.6E-01	8.6E-03	7.0E-02	2.2E-01	7.5E-03	6.1E-02	1.9E-01
Scattering σ [mrad]	69.0+/- 0.2	224+/- 5	*	54.8+/- 0.2	160+/- 7	*	46.9+/- 0.2	161+/- 8	*
Ratio σ/θph	2.7	8.8	*	2.7	7.8	*	2.8	9.5	*
LiF111 Crystal									
Ratio (t/CSDA Range)	3.6E-02	3.1E-01	9.8E-01	3.0E-02	2.6E-01	8.1E-01	2.6E-02	2.2E-01	7.0E-01
Scattering σ [mrad]	105.2+/- 0.1	350+/- 91	*	84.69+/- 0.06	500+/- 100	*	70.39+/- 0.07	250+/- 40	*
Ratio σ/θph	4.1	13.7	*	4.1	22.5	*	4.1	14.9	*

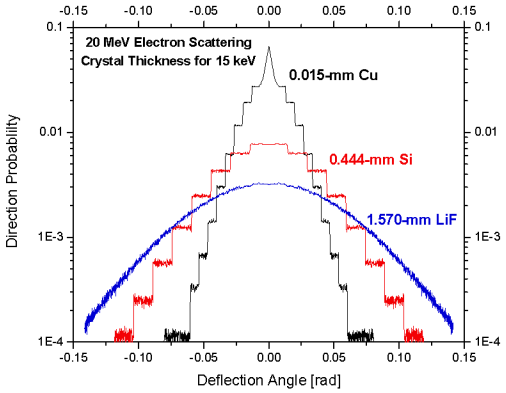

FIGURE 2. Angular distribution of simulated 20-MeV electron scattering in PXR targets with thickness, t, of one absorption length, L_a, for 15 keV PXR in the Cu, Si, and LiF targets. Note: the steps in the graphs are due to angular discretization in MCNPX.

CONCLUSIONS

This study demonstrates potential for PXR medical applications. First, the first Cu111 PXR was experimentally realized and with such metallic crystals optimized thickness may allow for a durable PXR target crystal that can withstand the high electron beam currents necessary for imaging applications. Second, since PXR is quasi-monochromatic, patient exposure to low energy photons can be reduced. In the simple model used here, the dose to mammography patients is reduced by a factor of 2. Finally, use of low energy electron accelerators down to 20 MeV show some promise. Lower PXR energies are preferred since they require thinner crystals. For all energies considered, the thinner Cu target crystal showed the most potential because of its small thickness compared to the LiF and Si crystals. Future work includes the use of the scattering information to calculate the absolute PXR yield using electron energies of 20-30 MeV and to conduct PXR experiments using a low energy port (18-24 MeV) at the RPI LINAC.

ACKNOWLEDGMENTS

Special thanks is given to Peter Brand and his staff at the RPI LINAC Facility. The experimental work on this project could not be done without their help. Additional appreciation goes to the Department of Physics, United States Military Academy for sponsoring travel to the CAARI Conference.

REFERENCES

1. P. Rulhusen, X. Artur, P. Dhez. *Novel Radiation Sources using Relativistic Electrons, from infrared to X-rays.* Singapore: World Scientific Series on Synchrotron Radiation Techniques and Applications, Vol. 4, 1998.
2. I.D. Feranchuk, K.G. Batrakov, Nucl. Instr. and Meth. A **543**, 55-57 (2005).
3. National Institute of Health Website. Available at: http://www.nibib.nih.gov/Research/ProgramAreas/Xra
4. B. Sones, Y. Danon, R.C. Block, *Nucl. Instr. and Meth. B* **227**, 22-31 (2005).
5. A.V. Shchagin, V.I. Pritupa, and N. A. Khizhnyak, *Phys. Letters A*, **148,** 485-488 (1990).
6. E. A. Bogomazova, et. al., *Nucl. Instr. and Meth. B* **201**, 276-291 (2003).
7. Y. Adischev, et. al., *Nucl. Instr. and Meth. B* **201**, 114-122 (2003).
8. B. Sones, Y. Danon, R.C. Block, *Nucl. Instr. and Meth. A* **560**, 589-597 (2006).
9. Y. Hayakawa, et. al., "Present status of the parametric X-ray generator at LEBRA," Proceedings of the 1st Annual Meeting of the Particle Accelerator Society of Japan and the 29th Linear Accelerator Meeting in Japan, Aug 4-6, 2004 Funabashi Japan, access at www-linac.kek.jp/mirror/lam29.lebra.nihon-u.ac.jp/WebPublish/4B05.pdf.
10. T. Akimoto, et. al., *Nuc. Inst. and Meth. A* **459**, 78-86 (2001).
11. K. H. Brenzinger, *Phys. Rev. Letters* **79**, 2462-2465 (1997).
12. A.P. Potylitsin. "Influence of beam divergence and crystal mosaic structure upon parametric X-ray radiation characteristics." arXiv:cond-mat/9802279 v1, 26 Feb (1998).
13. B. Sones, Y. Danon, R. Block, American Nuclear Society 2005 Annual Meeting, San Diego, CA, ANS Transactions vol. 92, 648-650 (2005).
14. B. Sones, Y. Danon, American Nuclear Society 2008 Annual Meeting, Anaheim, CA, ANS Transactions vol. 98, 395-397 (2008).
15. A. Wolbarst, *Physics of Radiology*, Medical Physics Publishing, Madison, Wisconsin, 2000, p. 221.
16. Monte Carlo N-Particle Transport Code (MCNPX Ver. 2.5.0), Los Alamos National Laboratory, Los Alamos, New Mexico, 2005.
17. NIST ESTAR Website. Available at: http://physics.nist.gov/cgi-bin/Star/e_table.pl.
18. P. Keall, et. al., *Medical Physics*, **Vol. 30, No. 4,** 574-582 (2003).